Including the pyramid optical gains into analytical models

Romain Fetick, Vincent Chambouleyron, Cedric Taissir Heritier

AO4ELT7 - June 2023 - Avignon

Including the pyramid optical gains into analytical models

Romain JL Fétick[a,b], Vincent Chambouleyron[c], and Cédric Taissir Héritier[a,b]

[a]ONERA, DOTA, ONERA, F-13661 Salon cx Air – France
[b]Aix Marseille University, CNRS, CNES, LAM, Marseille, France
[c]University of California Santa Cruz, USA

ABSTRACT

Fourier-filtering wavefront sensors (WFS), such as the pyramid of Zernike WFS, are shown to be highly sensitive. They are becoming the baseline for future adaptive optics (AO) systems for astronomy. The next generation Extremely Large Telescopes (ELTs) will be equipped with such sensitive WFS. However the main drawback of these sensors is a quick loss of linearity when subject to strong turbulence residuals.

Two major methods can be identified to simulate the AO point-spread-function (PSF): the end-to-end simulation and the analytical model. The first one propagates random samples of phase screens through a fully simulated AO loop, it can thus reproduce fine spatial and temporal effects, inlcuding the WFS non linearities. The second method is based on analytical formulas that provide a quick simulation with a good understanding of the AO system (separation of the AO error terms) but require a linear response of the system.

We develop here a method to include the non linearities of the WFS into analytical formulas. It consequently improves the accuracy of the simulation and enables to describe with good accuracy Fourier-filtering WFS. We test our method against end-to-end simulations, and derive possible applications for AO system design or performance estimation.

Keywords: adaptive optics, wavefront sensor, optical gain

1. INTRODUCTION

Between theoretical developments and onsky operations, simulation is an important step in the knowledge of adaptive optics systems. Numerical simulations are important during the AO design phase to choose instrumental trade-offs and to predict nominal performances in given observation conditions. It is also necessary to correlate AO commissioning data with simulations to verify the quality of the delivered system. The numerical tools are also used in the exploitation of scientific data for PSF reconstruction or PSF estimation.

We might identify two major categories of simulation tools in AO, the end-to-end simulations and the analytical models.

Contact: romain.fetick@onera.fr

End-to-end models describe as finely as possible the AO loop. They generate random phase screens and propagate them between different simulated components such as the deformable mirror and the wavefront sensor. These methods can describe every speckle of the PSF evolving with time. The numerical simulation is temporally discretized at least at the AO loop frequency, typically 500 Hz to some kilo-Hertz. From this fine description, non linear effect arise, such as the wavefront sensor non linear response depending on the phase amplitude, or the closed loop response that may diverge at high controller gain. The drawback of these fine simulations is that they require high computation power and long computation time. For AO systems running at kilo-Hertz, one second of phase movement requires already 1000 iterations, each iteration itself requires one or multiple Fourier transforms. In the case of modulated WFS or systems with high number of actuators, the computation time increases dramatically. The end-to-end simulations are consequently well adapted to a comprehensive check of the AO design.

On the other side, the analytical methods rely assumptions to greatly simplify the full AO loop to a minor set of equations. The advantage is that the electromagnetic phase residual power spectral density (PSD) is split into different error terms, each described by an equation. The dependence of the AO error with the observing conditions is thus explicit. The error budget clearly makes to appear the dominant terms, that are the one to mitigate to increase the AO performances. These analytical tools are fast, require only few Fourier transforms, and do not scale in computation time with the modulation radius or the number of actuators. They are well adapted from small to large AO system. The major drawback of analytical models are the assumptions and hypothesis required to simplify the AO system to a set of equations. They need to be tested to be validated in normal operating conditions.

Sections 2 and 3 describe the analytical method and its numerical implementation, especially regarding the non-linear effect of the optical gains. Section 4 compares the analytical method with end-to-end simulations. Finally, Section 5 shows our method applied to pragmatic operations with AO and non-linear WFS.

2. THE ANALYTICAL PSD-BASED METHOD

2.1 Description of the AO point-spread-function

The long-exposure point-spread-function of the system is decomposed into a static (telescope) contribution and a turbulent contribution (AO residuals) [10, 2], which gives

$$h = h_{\text{static}} \star h_{\text{AO}} \tag{1}$$

where h is the system PSF, h_{static} the static contribution, h_{AO} the AO residual PSF contribution, and $\star$ the convolution operator. The static PSF simply writes

$$h_{\text{static}} = \left|\mathcal{F}\left\{P e^{i\phi_{\text{static}}}\right\}\right|^2 \tag{2}$$

where $\mathcal{F}\{\cdot\}$ denotes the Fourier transform, P is the pupil aperture and ϕ_{static} the static phase map, including for example the non-common-path aberrations (NCPA) between the WFS and the scientific camera or non-zeros WFS reference (DM dark hole map).

The contribution of the residual phase to the long-exposure PSF writes [10]

$$h_{\text{AO}} = e^{-\sigma^2_{\text{total}}}\, \mathcal{F}^{-1}\left\{e^{\mathcal{F}^{-1}\{W_{\text{total}}\}}\right\} \tag{3}$$

where W_{total} is the residual phase power spectral density (PSD) and σ^2_{total} is the variance of the phase (the integral of the PSD). The computation of the PSF requires the computation of this PSD term, that depends on the AO system, the guide star and turbulence conditions.

Table 1. Error breakdown of an AO system

NAME	DESCRIPTION	THIS WORK
Fitting	Limited number of actuators in the pupil	Included
Temporal	Limited temporal bandwidth of the AO loop	Included
Photon	Photon noise (reconstructed onto the phase)	Included
RON	Readout noise (reconstructed onto the phase)	Included
Aliasing	Measurement aliasing due to WFS pixelisation	Not included
Anisoplanetism	Angular difference between the guide star and the object of interest	Not included

2.2 AO error breakdown on the phase PSD

The AO system performances is described through the AO error breakdown, that encompasses all possible sources of residual error on the electromagnetic phase. Table 1 summarises some of the common error terms for AO systems, the non-linearity of the WFS response is not included in the table since its effects are manifested on other terms (temporal and noise filtering errors) as we will describe is section 3.

The phase error terms are supposed independent one from the other, it is thus possible to add all their power spectral densities (PSD) such as

$$W_{\text{total}} = W_{\text{fitting}} + W_{\text{temporal}} + W_{\text{photon}} + W_{\text{RON}} \tag{4}$$

Each PSD term must now be explicitly written as a function of the observing conditions.

2.2.1 Fitting error term

The fitting error comes from the limited number of corrected modes in the pupil. If a total of N_m modes are corrected on a pupil of surface S, then it corresponds to an equivalent pitch of $p = \sqrt{S/N_m}$. The maximal corrected spatial frequency is then $f_{\text{corr}} = 1/(2p)$. The fitting error PSD writes

$$W_{\text{fitting}} = W_{VK}\,\overline{\mathcal{U}_{\text{corr}}} \tag{5}$$

where $\mathcal{U}_{\text{corr}}$ is the corrected AO area, that is equal to one for $f < f_{\text{corr}}$ and 0 otherwise. The non corrected area $\overline{\mathcal{U}_{\text{corr}}}$ is the complementary of $\mathcal{U}_{\text{corr}}$. The W_{VK} PSD is the turbulent PSD, assumed to be Von-Karman like

$$W_{VK}(f) = 0.023\, r_0^{-5/3} \left(1/L_0^2 + f^2\right)^{-11/6} \tag{6}$$

with r_0 the Fried parameter, L_0 the turbulent external scale and $f = \sqrt{f_x^2 + f_y^2}$ the spatial frequency.

2.2.2 Temporal error term

The AO loop is described through the formalism of feedback automatics systems such as

$$H_{CL}(f_t) = \frac{H_{OL}(f_t)}{1 + H_{OL}(f_t)} \tag{7}$$

where f_t is the temporal frequency, H_{CL} the feedback closed loop, and H_{OL} the open loop transfer function. This last term writes

$$H_{OL} = H_{WFS}\, H_{RTC}\, H_{DM} \tag{8}$$

with H_{WFS} is the temporal transfer function of the wavefront sensor (typically a frame integration at loop frequency F), H_{RTC} includes the RTC delay (pixel transfer, DM commands computation) and the controller (typically an integrator control law), and finally H_{DM} is the DM temporal transfer function. We assume the

DM has an infinite temporal bandwidth for sake of simplicity, it thus writes $H_{DM} = 1$. For a typical integrator controller, we obtain the transfer function

$$H_{OL} = \frac{1 - e^{-Tp}}{Tp} e^{-\tau p} \frac{g}{Tp} \tag{9}$$

where p is the Lapace variable, $T = 1/F$ the image integration time, τ the delay and g the integrator gain.

The turbulent PSD is filtered by the modulus squared of the temporal transfer function $|H_{CL}|^2$. The temporal and spatial frequencies are related as $f_t \longleftrightarrow V f_x$ for a wind along the X axis. It thus allows to filter a spatial PSD with a temporal filter. The temporal error PSD writes

$$W_{\text{temporal}} = W_{VK}\, \mathcal{U}_{\text{corr}}\, |H_{CL}(V f_x)|^2 \tag{10}$$

2.2.3 Photon and RON error terms

The photon noise and read-out noise are propagated into the AO loop thanks to the reconstructor. A non-regularised reconstructor writes as the inverse of the sensitivity of the WFS, called $\mathcal{S}_{WFS}(\phi)$, to a given spatial frequency (or to a given phase mode). The sensitivity of a non-linear WFS depends on the current phase ϕ. Using the convolutional formalism [5, 4], the sensitivity can be computed from the current PSF with respect to the calibration PSF h_{calib}. The average sensitivity thus relies on the average PSF h with respect to h_{calib}. The sensitivity is written as a function of the PSF such as $S_{WFS}(h, h_{\text{calib}})$.

The readout noise is propagated into the loop as [1]

$$W_{\text{RON}} = \frac{N_{\text{pix}} \sigma^2_{\text{RON}}}{N_\gamma^2} \frac{\mathcal{U}_{\text{corr}}}{S^2_{WFS}(h, h_{\text{calib}})} \frac{2}{F} \int_0^{F/2} |H_{\text{noise}}|^2 df_t \tag{11}$$

where N_{pix} is the number of pixels in one sub-pupil of the WFS camera, σ^2_{RON} is the readout noise variance, N_γ the number of photons per WFS frame and $|H_{\text{noise}}|^2$ the noise temporal filter. Similarly, the photon noise is propagated as [1]

$$W_{\text{photon}} = \frac{\sqrt{N_{\text{face}}}}{N_\gamma} \frac{\mathcal{U}_{\text{corr}}}{S^2_{WFS}(h, h_{\text{calib}})} \frac{2}{F} \int_0^{F/2} |H_{\text{noise}}|^2 df_t \tag{12}$$

with N_{face} the number of faces of the pyramid WFS.

3. INCLUDING THE OPTICAL GAINS

The optical gains are defined as the ratio of sensitivity between the calibration and the current operating point of the WFS. It writes

$$g_{\text{opt}} = \frac{S_{WFS}(h, h_{\text{calib}})}{S_{WFS}(h_{\text{calib}}, h_{\text{calib}})} \tag{13}$$

These gains are introduced in the transfer function of the system such as

$$H_{WFS,opt} = g_{\text{opt}}\, H_{WFS} \tag{14}$$

It modifies the temporal filtering of the loop and consequently the temporal error of Equation 10. We consequently see that the PSD terms W_{temporal}, W_{RON} and W_{photon} depend on the current PSF h through the WFS sensitivity and the optical gains. However the PSF h is computed from the PSD terms. A vicious circle of dependencies appears. We solve the issue with the following strategy (see Figure 1):

1. Assume the current PSF to be the calibration PSF, that is in our case the diffraction limit PSF. The current sensitivity is thus the calibration sensitivity, and consequently $g_{\text{opt}} = 1$. In other words, the WFS is assumed to work in its linear regime.

2. Compute the fitting error (Eq. 5), that does not depend on the optical gains.

3. Compute the temporal and noise PSD terms (Eq. 10, 11, 12), that depend on the sensitivity and the optical gains.
4. Compute the PSF from the PSD terms (Eq. 3)
5. Compute the sensitivity [4, 1] and the optical gains (Eq. 13)
6. Iterate on steps 3 to 5. Usually only three iterations are required to converge to a steady state.
7. Retrieve outputs of interest such as: PSF, error PSD terms, error variances (as the integral of the PSD), sensitivity map, optical gain map

The circle of dependencies between the PSF and the sensitivity is consequently solved by an iterative process on the steps 3 to 5 above. This solving method introduces the non-linearity of the WFS into the analytical method without using the computationally expensive end-to-end simulations. In practice we observe that only 3 iterations on the steps 3 to 5 are required to converge towards a steady state in terms of sensitivity maps, optical gains and PSF. The method is consequently fast and stable. The accuracy will be tested in the next section.

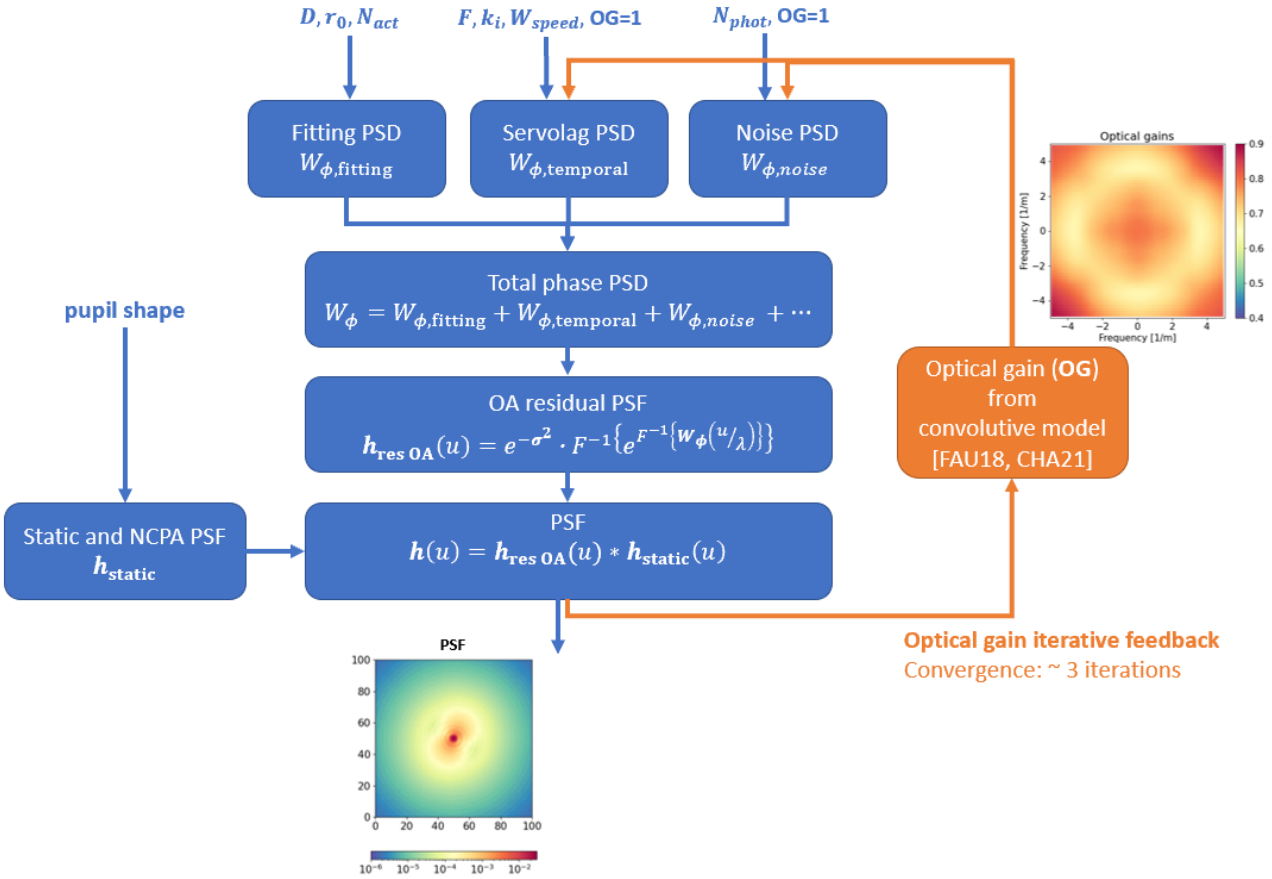

Figure 1. Iterative method used to compute the AO corrected PSF for a non linear WFS.

4. VALIDATION WITH OOPAO

The analytical PSD method is compared with the OOPAO (Object-Oriented Python Adaptive Optics) [7] end-to-end simulation software, that is the Python version of the legacy OOMAO [3] software in Matlab. OOPAO generates one or multiple phase screens sliding across the pupil in the Taylor frozen flow hypothesis. The

electromagnetic field is propagated between focal and pupil planes thanks to Fourier transforms. The software simulates deformable mirrors and wavefront sensors, including the modulated pyramid WFS.

Table 2. Simulation parameters

SYMBOL	DESCRIPTION	VALUE	UNIT
D	Telescope diameter	1.5	m
r_0	Fried parameter	12	cm
L_0	Turbulence external scale	30	m
V	Wind speed	3 or 8	m/s
$N_{\text{act}} \times N_{\text{act}}$	Number of actuators on the Cartesian grid	14×14	
N_m	Number of corrected modes	138	
M_V	Star magnitude in V band	0	
r_{mod}	PSF modulation radius	3	λ/D
F	Loop frequency	500	Hz
g	Integrator gain	0.3	
τ	Frame delay	$1/F$	s

Table 2 summarises the parameters used for the test simulation both in OOPAO and in our PSD based method. The OOPAO end-to-end tool was run over 4000 iterations of phase screens, each iteration representing a time step of $1/F$, the screen is moved at each step over a distance of V/F.

Two cases of wind speed are tested, a low wind at $V = 3$ m/s and a strong wind at $V = 8$ m/s. In the first case, the fitting error is dominant since $\sigma^2_{\text{fitting}} = 0.23$ rad^2 and $\sigma^2_{\text{temporal}} = 0.11$ rad^2. In the second case, the temporal error is dominant since its variance increases to $\sigma^2_{\text{temporal}} = 0.82$ rad^2. Results are shown on Figure 2. The analytical PSD method is able to provide the main structures of the PSF for both wind speed cases. The optical gains computed with our method are smaller with higher wind speed, as expected. The optical gains are not central-symmetric but show a strong cross pattern that is assumed to come from the pyramid edges aligned with the X and Y axis in our simulations. Table 3 shows the results in term of residual phase variances. The relative difference between our method and the full end-to-end simulation is less than 3% in the low wind case and less than 10% in the high wind case. In this last case, the residuals are high and might introduce strong non-linear effects that are not fully described by the convolutional model of the optical gains.

Table 3. Residual phase variance (rad^2) computed from the different simulations. The case without optical gain (no OG) allows to see the drop of performance due to the optical gains (with OG).

	$V = 3$ m/s	$V = 8$ m/s
OOPAO	0.33	1.14
This work (no OG)	0.32	0.83
This work (with OG)	0.34	1.04

5. APPLICATIONS

5.1 Optimal modulation abacus

According to the diversity of observing conditions, one might want to adapt the modulation radius to provide optimal AO performances. Indeed, in case of high SNR and poor turbulence conditions (high wind speed and small r_0), the WFS works better in a linear regime with high dynamic range, that is obtained for a high modulation radius. Reciprocally, low SNR and good atmospheric conditions require a sensitive WFS obtained at small modulation radius. The Figure 3 shows the optimal modulation radius to choose for a given AO system. In this case, it corresponds to the PAPYRUS [8, 6] AO system, whose main characteristics are a primary diameter

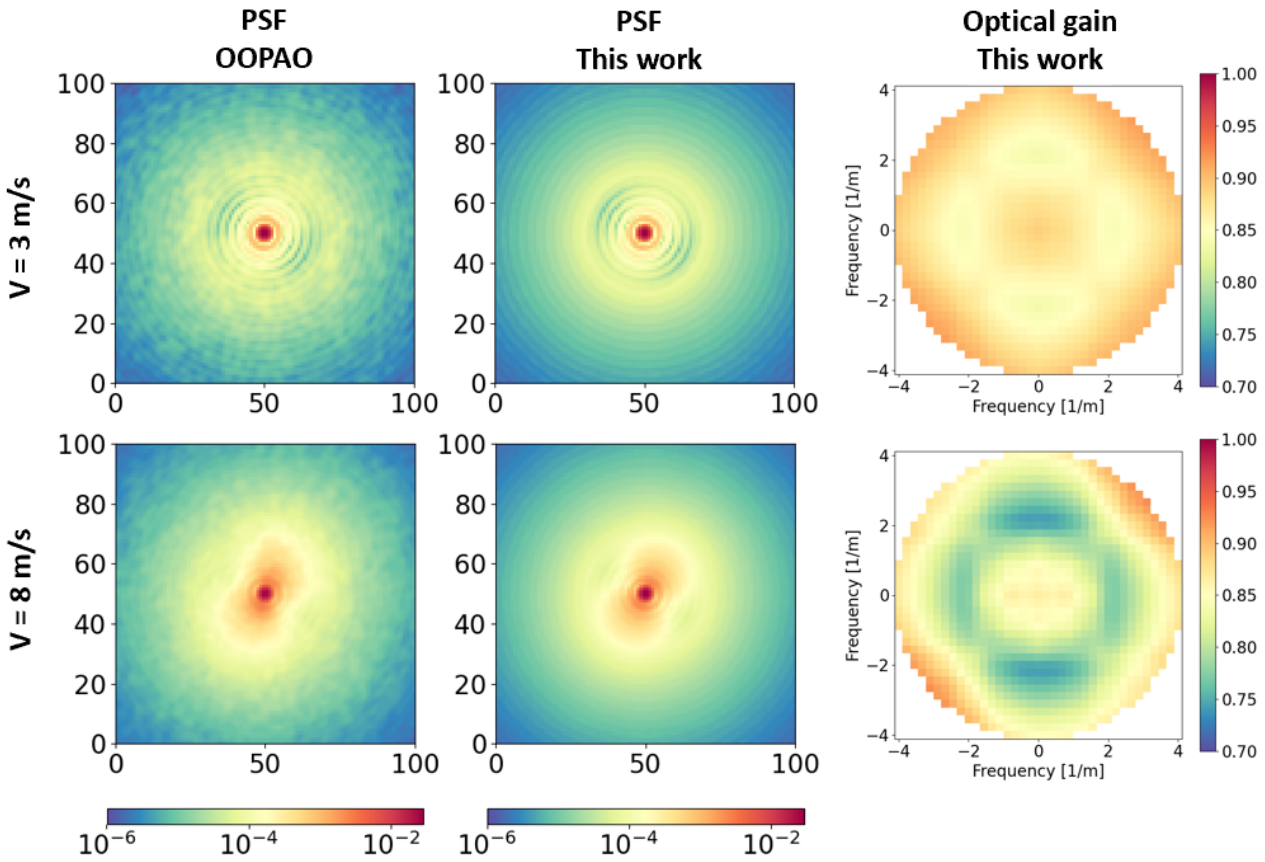

Figure 2. Results of the simulation for two cases of wind speed $V = 3$ m/s (top) and $V = 8$ m/s (bottom).

of $D = 1.52$ m, a DM with 17×17 actuators, a RTC running at $F = 500$ Hz and a modulated pyramid WFS working in the large visible band. The plots show the correct behaviour towards the observation parameters, where the sensitivity, *id est* low modulation radius, is required at low SNR and good turbulence conditions.

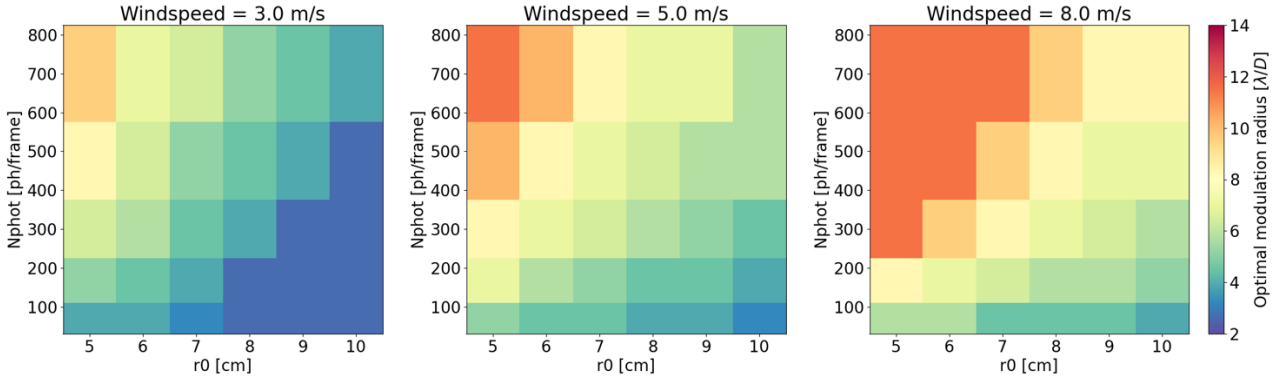

Figure 3. Optimal modulation abacus for a PAPYRUS like AO system, from low (left plot) to high (right plot) wind speed.

This kind of abacus can be plotted for each AO system and used during night operations. The AO system

should retrieve the wind speed, seeing condition and target magnitude to select the optimal modulation radius.

5.2 Extended object

Extended guide sources drastically lower the performances of Fourier filtering WFS. Indeed they correspond to an extra light modulation, as the sum of incoherent sources. Figure 4 (right plot) shows an elliptical extended object of 1 arcsec wide by 3.5 arcsec long, whereas the diffraction is $\lambda/D = 86$ mas and the modulation radius is $r_{\text{mod}} = 5\lambda/D$. The size of the object is thus much bigger than the AO modulation pattern. This introduces large extra modulation than lowers the optical gain down to 0.4 (left plot on the same Figure). This effect must be taken into account for a correct description of the WFS sensitivity. However end-to-end simulations have difficulties to deal with extended guide sources since they rely on a discretization of the object and perform one propagation per discretization point. It quickly leads to impressive amount of operations and computation time. These issues are solved by the convolutional model [9].

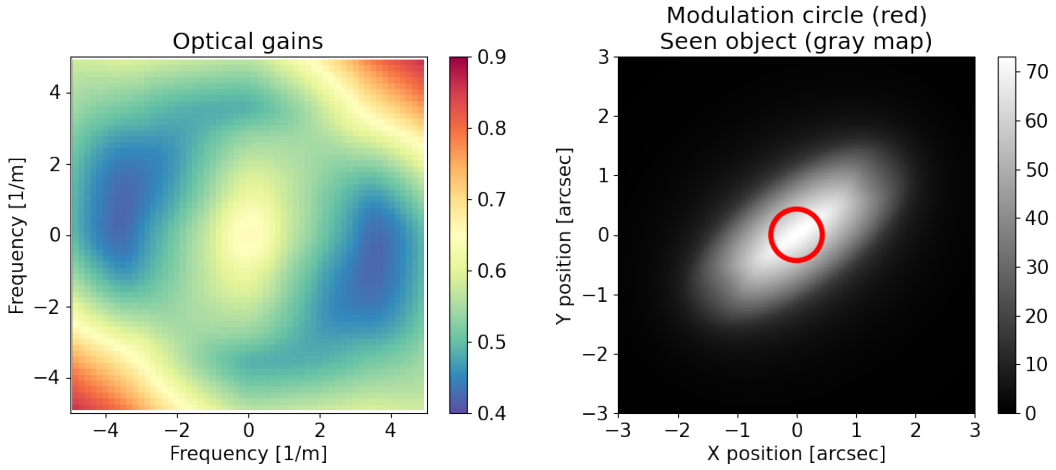

Figure 4. Optical gain (left) computed on a LGS like extended object (right).

6. CONCLUSION

We demonstrated the possibility to adapt the PSD analytical method to non linear WFS. It allows to estimate accurately the usual parameters of interest for an AO system, such as the PSF shape and its by-products which are the Strehl ratio and FWHM. Moreover the method allows to extract an error budget of the AO system, which is useful for AO design or operations to verify the dominant error terms. It makes it possible to tackle the bottlenecks of the AO system to increase its performances in specific operation conditions.

Even though this work is focused on the pyramid wavefront sensor, the method is applicable to any Fourier-filtering wavefront sensor, provided that the convolutional model is accurate enough to describe the non linear effects. Stronger effects, such as modal coupling at high residual turbulence cannot be described by such a method.

ACKNOWLEDGMENTS

This work benefited from the support of the the French National Research Agency (ANR) with WOLF (ANR-18-CE31-0018), APPLY (ANR-19-CE31-0011) and LabEx FOCUS (ANR-11-LABX-0013); the Programme Investissement Avenir F-CELT (ANR-21-ESRE-0008), the Action Spécifique Haute Résolution Angulaire (ASHRA) of CNRS/INSU co-funded by CNES, the ECOS-CONYCIT France-Chile cooperation (C20E02), the ORP-H2020 Framework Programme of the European Commission's (Grant number 101004719), STIC AmSud (21-STIC-09), the Région Sud and the french government under the France 2030 investment plan, as part of the Initiative d'Excellence d'Aix-Marseille Université -A*MIDEX, program number AMX-22-RE-AB-151.

References

[1] Vincent Chambouleyron. "Optimisation de l'analyse de surface d'onde par filtrage de Fourier pour les systèmes d'optique adaptative à hautes performances". Theses. Aix-Marseille Université, Dec. 2021. URL: https://hal.science/tel-03761481.

[2] Jean-Marc Conan. "Etude de la correction partielle en optique adaptative". PhD thesis. Paris 11, 1994.

[3] Rodolphe Conan and C Correia. "Object-oriented Matlab adaptive optics toolbox". In: *Adaptive optics systems IV*. Vol. 9148. SPIE. 2014, pp. 2066–2082.

[4] Olivier Fauvarque. "Optimisation des analyseurs de front d'onde à filtrage optique de Fourier". PhD thesis. Aix-Marseille, 2017.

[5] Olivier Fauvarque et al. "General formalism for Fourier-based wave front sensing". In: *Optica* 3.12 (Dec. 2016), pp. 1440–1452. DOI: 10.1364/OPTICA.3.001440. URL: https://opg.optica.org/optica/abstract.cfm?URI=optica-3-12-1440.

[6] Romain Fétick, Vincent Chambouleyron, Eduard Muslimov, et al. "PAPYRUS: one year of on-sky operation". In: *AO4ELT-7 proceedings*. 2023.

[7] Taissir Heritier-Salama. "OOPAO". In: *AO4ELT-7 proceedings* (2023).

[8] Eduard Muslimov et al. "Current status of PAPYRUS: the pyramid based adaptive optics system at LAM/OHP". In: *Optical Instrument Science, Technology, and Applications II*. Vol. 11876. SPIE. 2021, pp. 56–68.

[9] Francisco Oyarzun, Vincent Chambouleyron, et al. "Pyramid wavefront sensor with laser guide star: Photon noise and convolutional model". In: *AO4ELT-7 proceedings*. 2023.

[10] François Roddier. "The effects of atmospheric turbulence in optical astronomy". In: *Progress in optics*. Vol. 19. Elsevier, 1981, pp. 281–376.